TECHNICAL ARTICLE

# Microstructure, Corrosion Resistance, and Hardness of Simulated Heat-Affected Zone of Duplex UNS S32205 and Superduplex UNS S32750 Stainless Steels

*P.H.R. Pecly, B.B. Almeida, G. Perez, A.R. Pimenta, and S.S.M. Tavares*

**Thermal simulation is an interesting method to reproduce different regions of the heat-affected zone (HAZ) in specimens with dimensions proper to perform microstructural investigations, corrosion resistance and mechanical tests. In this work, different regions of the HAZ of duplex UNS S32205 and superduplex UNS S32750 stainless steels were reproduced using a Gleeble machine. For each material, thermal cycles with peak temperatures of 800, 1000, 1200 and 1350 °C were reproduced in order to evaluate the microstructure, pitting resistance, hardness and microhardness of the phases. It was found that the critical pitting temperature (CPT) was reduced in specimens processed with a peak temperature of 1350 °C in comparison with the base metals, while with peak temperatures of 800 and 1000 °C there was an increase in the CPT. Secondary austenite precipitation was identified in specimens with peak temperatures 800 and 1000 °C, but this phase did not impar the pitting resistance. Intense chromium nitrides precipitation and increase in the ferrite phase content were the main microstructural changes observed with peak temperature 1350 °C. The duplex steel undergone higher ferritization than the superduplex. The CPT was reduced with the chromium nitride precipitation, but the microhardness of the ferrite was not affected by these particles.**

## 1. Introduction

Duplex (DSS) and superduplex (SDSS) stainless steels are corrosion-resistant alloys (CRAs) with growing demand in different sectors, from construction to nuclear industries. In special, these materials are largely used in oil and gas (offshore), pulp, pharmaceutical, chemical, food and beverage industries (Ref 1-3). It's well known that the optimum corrosion resistance and mechanical properties of these materials are obtained with a microstructure of about equal parts of ferrite ($\alpha$) and austenite ($\gamma$) and free of other phases and micro-constituents (Ref 1-3). However, due to the difficulty of obtaining the best austenite/ferrite proportion (1:1), in the welded joint regions (Ref 4, 5), heat-treated base metal and thermo-

mechanical operations, the standards establish some ranges for the ferrite content, as shown in Table 1.

Failures due to improper microstructures of duplex and superduplex stainless steels are described in the literature (Ref 9-16). Hitchcock (Ref 9) studied the failure of a forged downhole tool of a SDSS due to sigma ($\sigma$) phase formation as a consequence of an inadequate solution heat treatment. Smiderle et al. (Ref 10) investigated the failure of a SDSS pipe for seawater handling at room temperature, which is unexpected for this type of material. The pipe had a microstructure containing a high percentage of sigma phase, probably resulting from inadequate heating of the pipe to assembly in the correct position for welding. On the other hand, welds without sigma phase, but containing a high density of nitrides and carbides are also prone to fail in service. Linton et al. (Ref 11) studied the failure by chloride stress corrosion cracking of a pressure vessel of superduplex stainless steel UNS S32750 designed to strip vinyl chloride monomer. This failure occurred by a combination of localized corrosion and stress corrosion cracking (SCC) and was associated with welded joints.

The use of DSSs and SDSSs often requires welding for joining plates or pipes. These materials can be welded by almost all arc processes, such as SMAW, GMAW, GTAW and SAW, but some care must be taken to avoid improper microstructures (Ref 3, 12-17). A great challenge is to obtain a $\alpha$:$\gamma$ proportion close to 1:1 or at least within the ranges specified (see Table 1). So important as the correct $\alpha$:$\gamma$ proportion is to avoid the formation of intermetallic phases, such as $\sigma$ and chi ($\chi$) phases. Pezzato et al. (Ref 18) reported the decrease in critical pitting temperatures (CPT) of lean duplex, duplex and superduplex steels due to deleterious precipitation of secondary austenite ($\gamma_2$), nitrides, and intermetallics $\sigma$ and $\chi$ phases. The kinetics of precipitation of these phases is

**P.H.R. Pecly**, Programa de Pós-graduação em Engenharia de Montagem Industrial, Universidade Federal Fluminense, Niterói, Brazil; **B.B. Almeida** and **G. Perez**, Programa de Pós-graduação em Engenharia Mecânica (PGMEC), Universidade Federal Fluminense, Niterói, Brazil; **A.R. Pimenta**, Programa de Pós-graduação em Engenharia de Montagem Industrial, Universidade Federal Fluminense, Niterói, Brazil; and LISComp, Instituto Federal do Rio de Janeiro, Paracambi, Brazil; and **S.S.M. Tavares**, Programa de Pós-graduação em Engenharia de Montagem Industrial, Universidade Federal Fluminense, Niterói, Brazil; and Programa de Pós-graduação em Engenharia Mecânica (PGMEC), Universidade Federal Fluminense, Niterói, Brazil. Contact e-mail: ssmtavares@id.uff.br.

**Table 1  Requirements regarding the ferrite content in base metal, heat-affected zone (HAZ) and weld metal (WM)**

| Standard | Ferrite content | | |
| --- | --- | --- | --- |
| | Base metal, % | HAZ, % | Weld metal, % |
| API RP 582 (Ref 6) (API TR 938C (Ref 7)) | 30-65 | 30-65 | 30-65 |
| NORSOK M630 (Ref 8) | 30-65 | 30-65 | 30-65 |
| OIL and gas specifications (Ref 5) | 35-55 | < 60-65 | < 60 |

enhanced by the increase in ferritizing elements, such as Cr, Mo, W and Si. As a consequence, SDSSs are more susceptible to corrosion decay and embrittlement due to intermetallics ($\sigma$ and $\chi$) than DSSs. In welded joints, the intermetallic phases are favored by the increase in heat input and interpass temperature, which decreases the cooling rate of heat-affected zone (HAZ) and weld metal (WM). On the other hand, rapid cooling of weld, such as found in thin wall tubes and plates is also undesirable because it provokes an excess of ferrite and intense chromium nitrides ($CrN$ or $Cr_2N$) precipitation inside the ferrite grains and in the $\alpha/\gamma$ boundaries (Ref 3, 15-17, 19, 20). Gennari et al. (Ref 21) measured a lower CPT in in the weld metal (WM) in relation to the base metal (BM) of superduplex steel, and associated this result to the higher ferrite content found in the WM.

Generally, the HAZ can be defined as a region from the base metal, adjacent to the weld metal, which suffered changes in microstructure and properties due to the thermal cycle imposed by welding. In practice, for a wide range of welding operations in DSSs and SDSSs, the HAZ is a very narrow region, which can be divided into subregions, according to the peak temperature achieved. In this sense, the use of thermal simulators, such as Gleeble machines, can be used to produce samples with thermal cycles typical of HAZ. These samples have a larger size than the HAZ produced by welding and can be used to study the effects of thermal cycles on the microstructure and properties. The work of Morales et al. (Ref 22) used the thermal simulation to study the morphology of austenite, the precipitation of Cr nitrides and corrosion resistance of the heat-affected zone of DSS USN S31803. Hsieh et al. (Ref 23) used samples of simulated HAZ to study the influence of cooling time from 800 to 500 °C ($\Delta t_{8/5}$) on the microstructure and corrosion resistance of specimens of 22%Cr-3%Mo DSSs with different N, Ni, and Mn contents.

The goal of this work was to characterize the microstructure and corrosion resistance of simulated heat-affected zones of duplex (UNS S32205) and superduplex (UNS S32750) stainless steels with different peak temperatures ($T_P$). The samples produced in the Gleeble machine are sufficiently large to characterize the corrosion resistance and microhardness of the phases, and the results can be associated to micro-regions of real welded joints. The corrosion resistance was evaluated by measurements of the critical pitting temperature (CPT) and cyclic polarization tests. The hardness and microhardness of phases were correlated to microstructure features. Also, the behavior of the simulated of HAZ of both steels was compared.

## 2. Materials and Methods

The materials analyzed in this work were from hot extruded seamless pipes of duplex (UNS S32205) and superduplex (UNS S32750) stainless steels, both with 114.5 mm of external diameter and 6.02 mm of thickness (schedule 40). They will be referred to S32205 and S32750 in this work. Table 2 shows the chemical composition of both steels. Chemical analysis was made using the combustion method for C, S, and N and optical emission spectroscopy (OES) for other elements.

Specimens with dimensions $105 \times 10 \times 4.5$ mm were cut and machined. They were submitted to thermal simulations in a Gleeble 3800 machine. Different regions of the HAZ were simulated in both materials, adopting four different peak temperatures: 1350, 1200, 1000 and 800 °C. An interval of five seconds in the peak temperature was programmed. The thermal cycles are in correspondence with the Rykalin-2D model (Ref 25). Experimental plots of temperature *versus* time were obtained with data collected by thermocouples spot welded in the specimens. As an example, Fig. 1 shows the thermal cycles of the S32205 steel.

The free span is the region of the specimen submitted to the thermal cycle. The length of this region depends on the simulation parameters. In this work, the estimated free span was 44.0 mm (Fig. 2). Specimens from this area were cut for the microstructural analysis, corrosion tests and microhardness tests.

Microstructural analyzes were performed in light optical (LOM) and scanning electron (SEM) microscopes. The specimens were etched with Behara's solution (80 ml $H_2O$, 20 ml HCl and 0.3 g of potassium metabisulfite) for phase quantification by quantitative metallography. Electrolytic etching with 10-15%NaOH solution (3 V, 15-60 s) was used to reveal the phases for microhardness measurements with Vickers method with 0.245 N (25 gf) of load. The microhardness was measured in each phase (ferrite and austenite). Eight measurements for each phase were made for each specimen. Electrolytic etching with 10% oxalic acid solution (9 V, 60 s) was performed to qualitatively evaluate the Cr nitrides precipitation. For the SEM analysis with backscattered electrons image, the specimens were finished by mechanical polishing with diamond paste 1.0 $\mu$m, without etching.

Vickers hardness was measured in each sample with 98.07 N (10 kgf) of load. Eight points for each sample were analyzed.

**Table 2  Chemistry composition of UNS S32205 and UNS S32750 (wt.%)**

| | UNS S32205 | | UNS S32750 | |
|---|---|---|---|---|
| Element | Standard (Ref 24) | Chemical analysis | Standard (Ref 24) | Chemical analysis |
| C | 0.030 (máx.) | 0.015 | 0.030 (máx.) | 0.016 |
| Si | 1.00 (máx.) | 0.50 | 0.80 (máx.) | 0.25 |
| Mn | 2.00 (máx.) | 0.86 | 1.20 (máx.) | 0.56 |
| P | 0.030 (máx.) | 0.025 | 0.035 (máx.) | 0.021 |
| S | 0.020 (máx.) | < 0.0005 | 0.020 (máx.) | 0.0007 |
| Cr | 22.0-23.0 | 22.25 | 24.0-26.0 | 25.55 |
| Ni | 4.5-6.5 | 5.36 | 6.0-8.0 | 6.40 |
| Mo | 3.0-3.5 | 3.15 | 3.0-5.0 | 3.86 |
| Cu | … | … | 0.5 (máx.) | 0.15 |
| N | 0.14-0.20 | 0.173 | 0.24-0.32 | 0.287 |
| Fe | Balance | Balance | Balance | Balance |
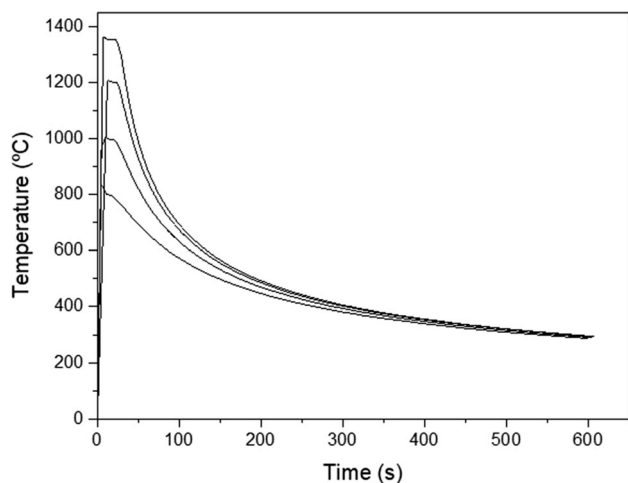


**Fig. 1** Thermal cycles of specimens of duplex stainless steel with peak temperatures 800, 1000, 1200 and 1350
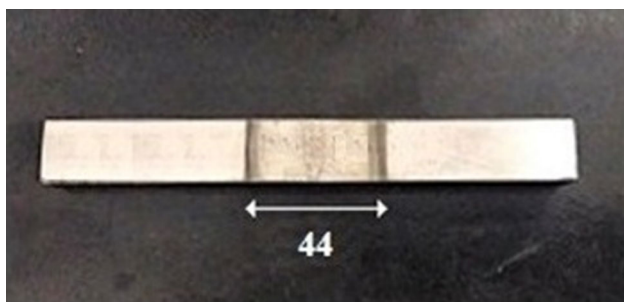


**Fig. 2** Free span region in the specimen submitted to thermal simulation

The critical pitting temperature (CPT) was measured using the potentiostatic method described in the ASTM G-150 (Ref 26). The three-electrode cell was assembled with a working electrode (WE), a saturated calomel electrode (SCE) as reference, and a Pt wire as counter-electrode (CE). The WEs were constructed with the specimen embedded in epoxy resin with a copper wire accomplished for electric contact. The surface of the WEs was prepared by grinding with emery papers 100, 220, 300 and 400 grit. The WE potential was maintained at 700 mV (anodic), and the temperature was increased at a rate equal to 3 °C/min. The CPT was the temperature at which the current density achieved 100 $\mu$A/cm$^2$ and maintained above this value for more than 60 s. Three tests per condition were performed. Specimens of both steels processed in the Gleeble were also submitted to cyclic polarization test in 3.5% NaCl solution at a temperature higher than the CPT measured. In this test, after the stabilization of the open circuit potential for 1 h, the potential was increased with a sweep rate of 1.0 mV/s. When the current density increased and achieved 5.0 mA/cm$^2$ the potential scanning was reversed to the cathodic direction. After the polarization tests the specimens were polished and etched with Behara's solution for observation in the LOM.

## 3. Results and Discussion

Figure 3(a) and (b) shows the microstructure of both steels, as received, the so-called base metals. Austenite islands with secondary austenite within the ferrite matrix are observed, with ferrite volume percentages of 54.2 ± 11.2% in the DSS S32205 and 46.9 ± 9.5% in the SDSS S32750.

Figures 4(a-d) and 5(a-d) show the LOM images of specimens of S32205 and S32750, respectively, processed in the Gleeble with peak temperatures of 800 °C, 1000 °C and 1200 °C. In these images, the ferrite grain boundaries were revealed, and intergranular secondary austenite ($\gamma_2$) particles were observed. Some austenitic islands partially ferritized are observed in both steels processed with $T_P$ = 1200 °C, as shown in circled areas of Fig. 4(c) and 5(c). Figures 4(d) and 5(d) show the intergranular $\gamma_2$ particles with more detail in specimens processed with $T_P$ = 1200 °C.

The microstructure of S32205 and S32750 specimens processed with a peak temperature of 1350 °C are shown in Fig. 6(a) and (b) and 7(a) and (b), respectively. It is clearly observed the increase in the ferrite content in both steels, but more pronounced in the S32205 steel. In this steel, Widmanstätten austenite (WA), intergranular austenite (IA) and grain boundary austenite (GBA) were observed, while in the superduplex S32750 intergranular $\gamma_2$ (IA-$\gamma_2$) and partially dissolved primary austenite are predominant in the microstructure. The results of phase quantification are presented in
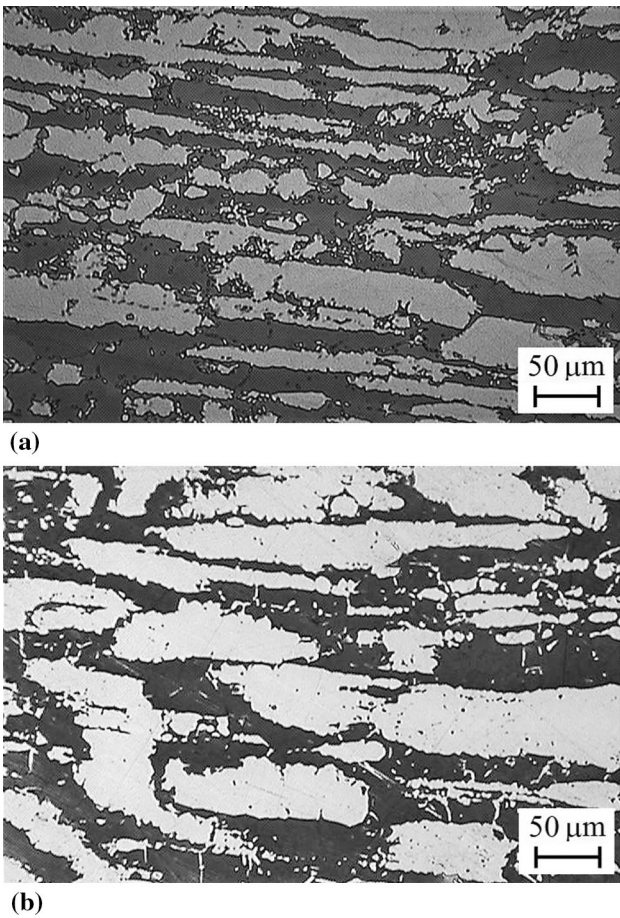
**Fig. 3** Microstructures of base metals: (a) S32205; (b) S32750

Table 3. The excessive ferrite content is a serious problem in SDSS and DSS because it results in large ferrite grains and intense chromium nitride precipitation (Ref 15–17). Colonies of chromium nitrides inside the ferrite grains were revealed with Behara's etching in specimens processed with $T_P$ = 1350 °C, and are shown in Fig. 6(b) and 7(b). Figure 8(a-d) shows the specimens processed with $T_P$ = 1200 °C and 1350 °C, etched with 10% acid oxalic solution (9 V, 60 s). This etching can be used to detect and qualitatively evaluate the chromium nitrides precipitation (Ref 27), and is more effective for this purpose than Behara's etching. As a result, it was observed that specimens processed with $T_P$ = 1200 °C also presented some chromium nitrides inside the ferrite grains. On the other hand, specimens with $T_P$ = 1350 °C, with a high density of Cr nitrides in the ferrite, also presented microcracks associated to nitride precipitation, as shown in the SEM images of Fig. 9(a) and (b). Such microcracks were observed in a previous work (Ref 17) and were found to be a kind of stress corrosion cracking provoked by the etching with oxalic acid solution and the lattice tension.

Using the WRC-1992 formulae (Ref 28), the $Cr_{eq}/Ni_{eq}$ is 2.72 for the S32205 steel, and 2.31 for the S32750 steel. The higher ferrite content observed in the specimens of S32205 is correlated to its higher $Cr_{eq}/Ni_{eq}$ ratio, which means that the ferrite solvus temperature for the SDSS S32750 is higher than for the DSS S32205, or the tendency to ferritization is higher for the S32250 than for the S32750 (Ref 28). On the other hand, the higher Cr and Mo contents of the S32750 steel make
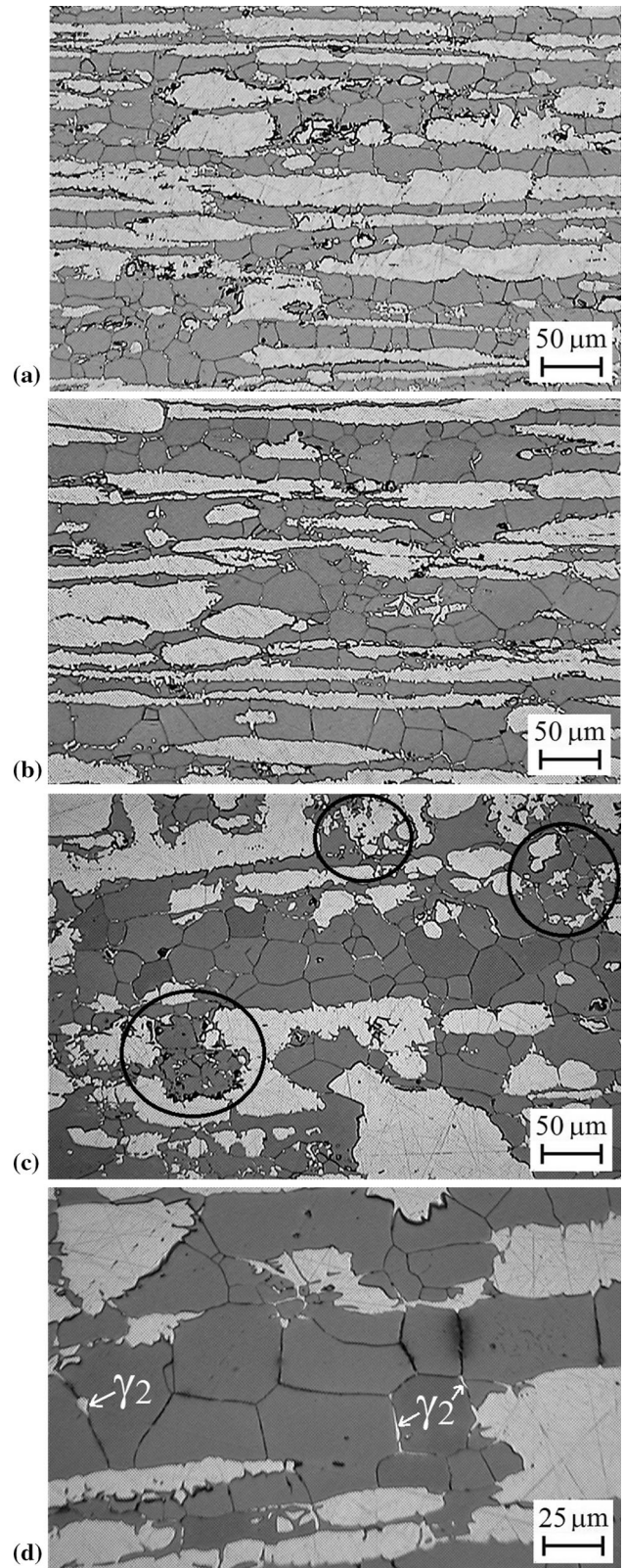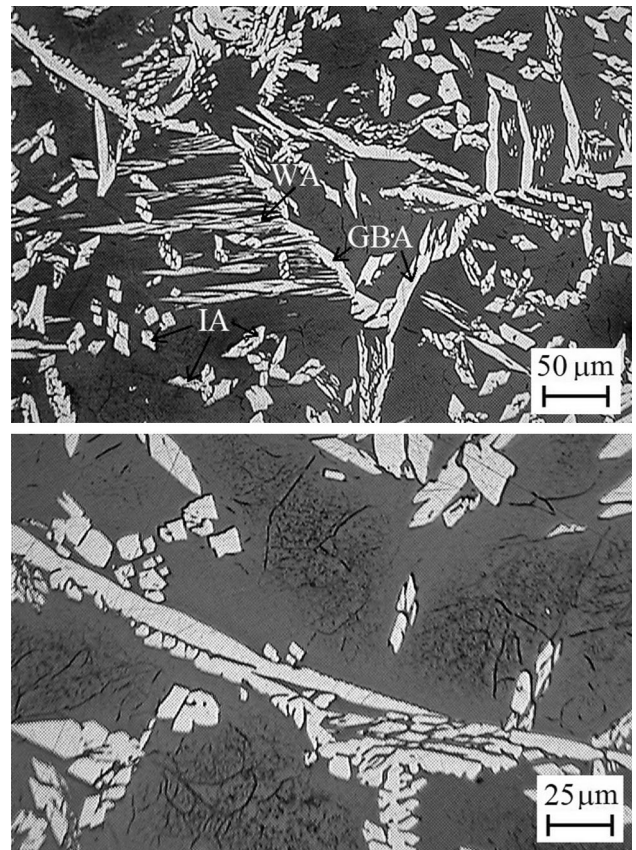


**Fig. 4** Microstructures of specimens of S32205 processed in the Gleeble with (a) $T_P$ = 800 °C; (b) $T_P$ = 1000 °C; (c) and (d) $T_P$ = 1200 °C

it more susceptible to intermetallic phases precipitation than S32205 (Ref 28). The risk of intermetallics formation increases if practices with high heat input and pre-heating are employed.

(a)

(b)

(c)

(d)
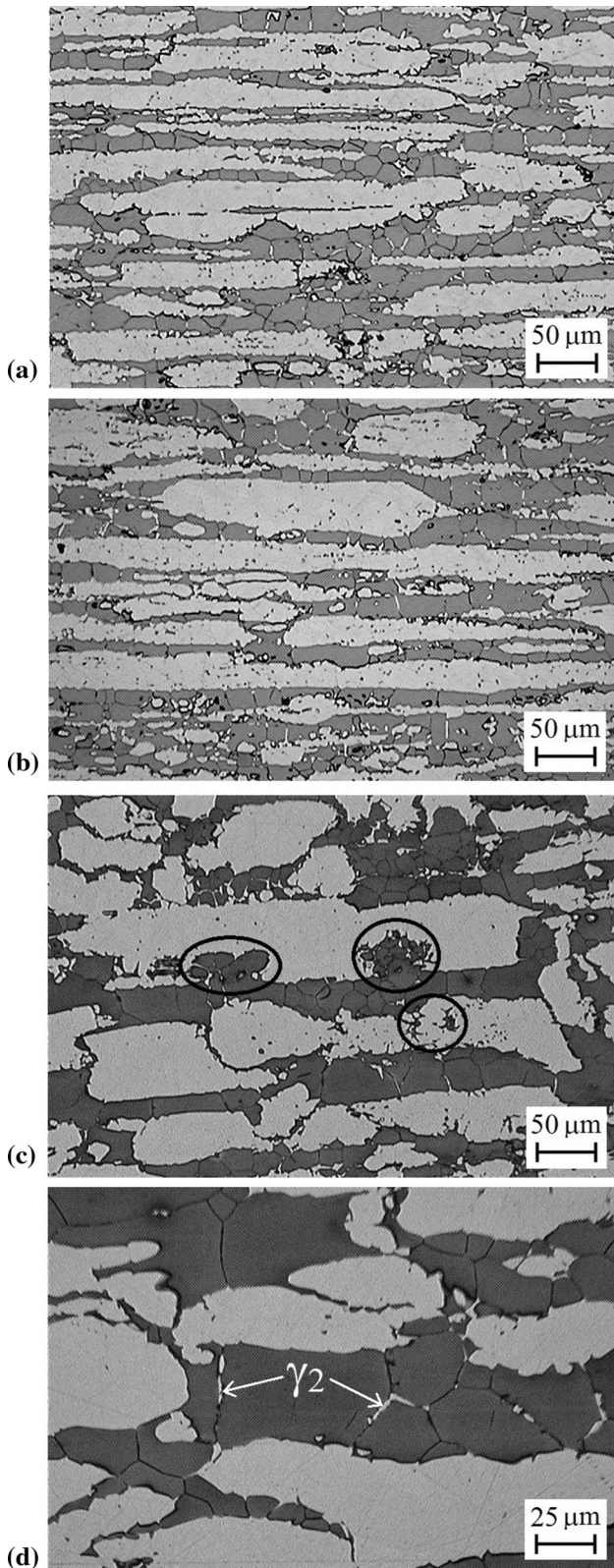
**Fig. 5** Microstructures of specimens of S32750 processed in the Gleeble with (a) $T_P$ = 800 °C; (b) 1000 °C; (c) and (d) 1200 °C



**Fig. 6** Specimens of S32205 steel processed with $T_P$ = 1350 °C

**Table 3 Ferrite contents of base metals and specimens processed in the Gleeble**

| $T_P$, °C | S32205 | S32750 |
|---|---|---|
| Base metal | 54.2 ± 11.2 | 46.9 ± 9.5 |
| 800 | 48.9 ± 9.0 | 44.5 ± 10.0 |
| 1000 | 51.1 ± 9.0 | 44.1 ± 10.0 |
| 1200 | 55.2 ± 2.0 | 52.6 ± 3.3 |
| 1350 | 62.5 ± 6.2 | 55.4 ± 4.1 |

According to Gunn (Ref 3), the cooling time from 1200 to 800 °C ($\Delta t_{12/8}$) must be between 4 and 15 s, or the cooling rate in this interval must be in the 20-50 °C/s interval. Analyzing the thermal cycles imposed in this work (Fig. 2), the $\Delta t_{12/8}$ and the cooling rate were out of the ranges recommended by Gunn (Table 4). Detailed analyzes by SEM of both steels processed with $T_P$ = 1200 and 1350 °C were performed to search for intermetallics. The specimens were prepared by polishing, without etching, and observed in the backscattered electrons (BSE) mode. This procedure was successfully used to evaluate the presence of Mo-rich $\sigma$ and $\chi$ phases in previous works, since these phases are heavier and appear lighter than austenite and ferrite (Ref 29, 30). The investigation did not reveal other phases than ferrite and austenite, and some examples of the microstructures observed in the BSE mode are shown in Fig. 10(a) and (b). It can be concluded that the limit of 15 s for the $\Delta t_{12/8}$ is conservative. In fact, although the sigma phase is the most studied intermetallic phase in the physical metallurgy of duplex stainless steels, its appearance as a consequence of welding is rarely reported in the literature. Up to now, the failures of duplex and superduplex stainless steels caused by embrittlement due to sigma phase are more frequently associ-
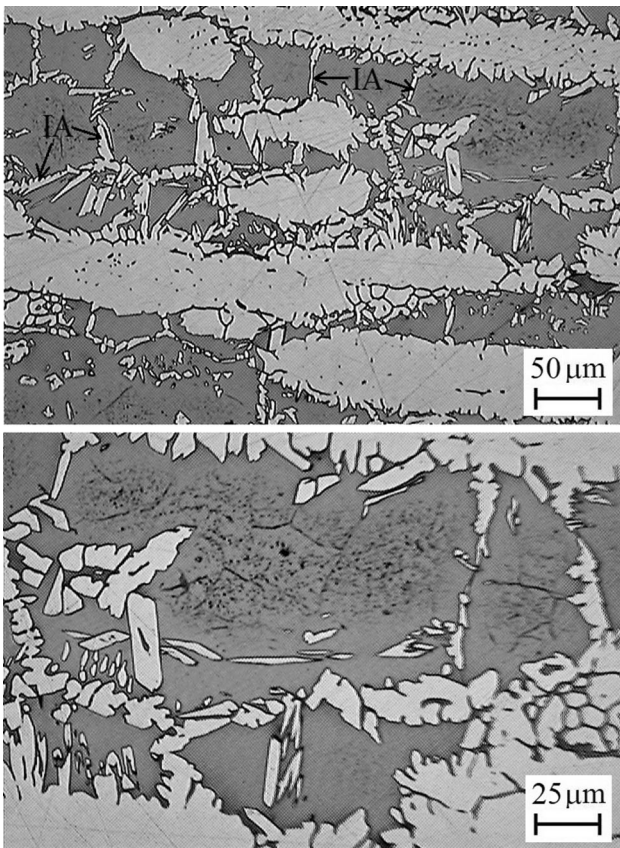
**Fig. 7** Specimens of S32750 steel processed with $T_P$ = 1350 °C

ated to inadequate practices of thermomechanical or heat treatments (Ref 9, 10) than to welding operation.

An interesting behavior was found in studying the hardness and microhardness of austenite and ferrite phases, as shown in Fig. 11(a) and (b). As expected, the hardness values of S32750 are slightly superior to the S32205, but both steels show the same trends. Microhardness of austenite is superior to the ferrite in all processing conditions, which can be attributed to the high nitrogen content of the austenite. In the specimens processed with $T_P$ = 1350 °C the intense $CrN/Cr_2N$ precipitation does not increase the microhardness of the ferrite phase, as can be also observed in Fig. 12. This result confirms the findings of Conceição et al. (Ref 27), but is in disagreement with other previous works that claims for precipitation hardening effect of Cr nitrides particles (Ref 31, 32).

It is also worth noting that the hardness values are higher than the individual microhardness of the phases, which means that grain boundaries play an important role in the mechanical resistance of duplex and superduplex steels.

Figure 13 shows the critical pitting temperature (CPT) as a function of the $T_P$. Both steels present a similar behavior, with the S32750 showing higher CPT, as expected. First, the CPT was increased in specimens processed with peak temperatures of 800 and 1000 °C. The main microstructural change in these specimens was the precipitation of intergranular $\gamma_2$, which does not explain the increase in CPT. It is possible that the re-heating at 800 and 1000 °C have promoted the redistribution of Cr by diffusion, eliminating or reducing the chemical composition gradients present in the base metal. Similar behavior was reported in superduplex steels UNS S32750 and UNS S32760
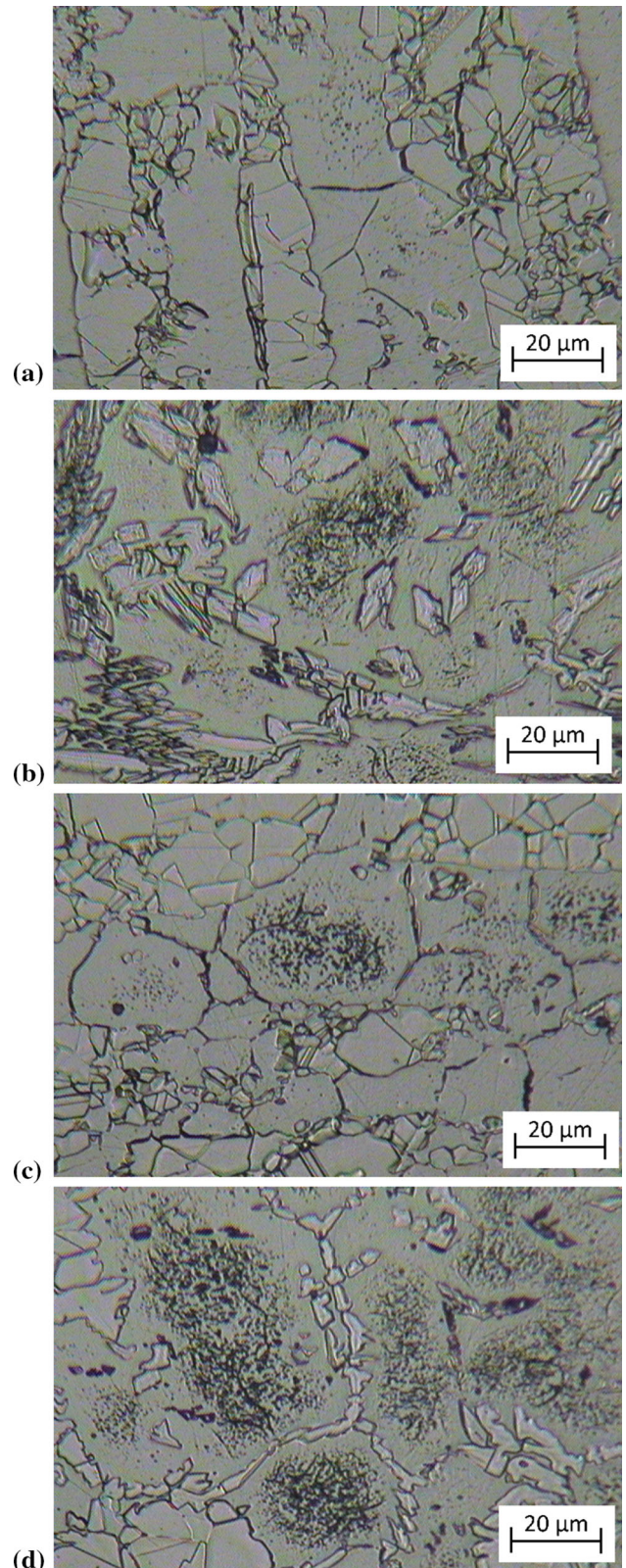


**Fig. 8** LOM images of specimens processed with $T_P$ = 1200 °C and 1350 °C: (a) S32205, $T_P$ = 1200 °C; (b) S32205, $T_P$ = 1350 °C; (c) S32750, $T_P$ = 1200 °C; (d) S32750, $T_P$ = 1350 °C

submitted to aging at 475 °C (Ref 33). The CPT increased with aging for 8 h and then decreased for higher aging time. On the other hand, specimens processed with peak temperature higher
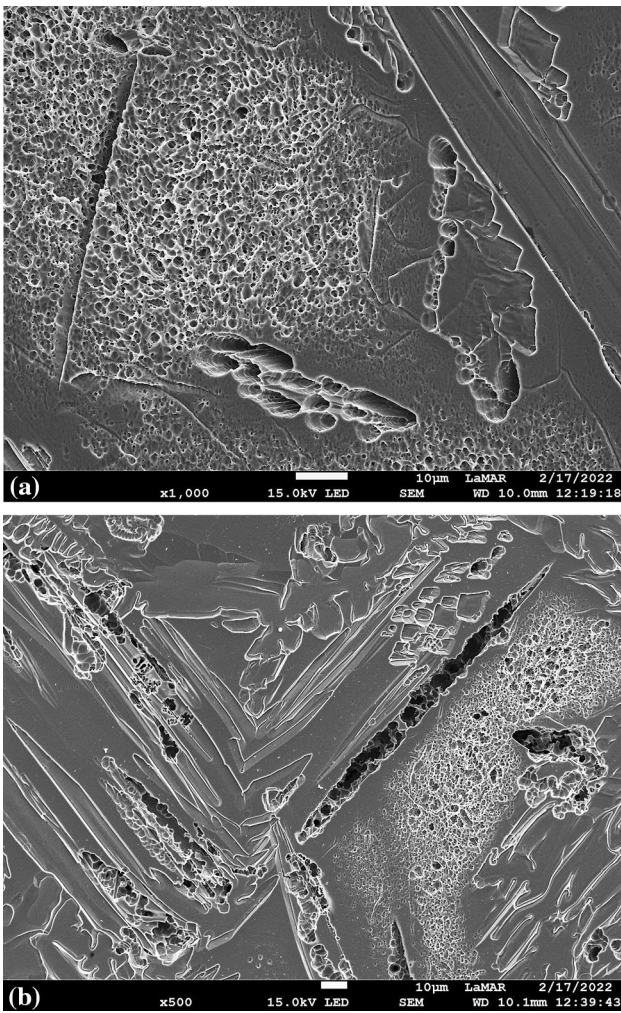
**Fig. 9** SEM images of specimens processed with $T_P = 1350\ °C$ etched with 10% acid oxalic solution (9 V, 60 s): (a) S32205; (b) S32750
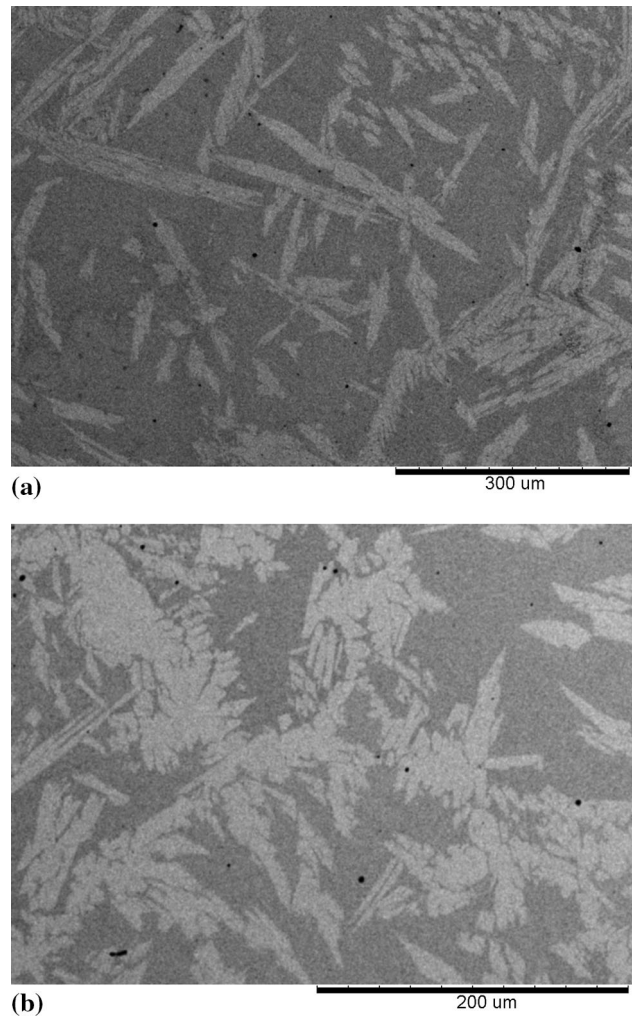


**Fig. 10** SEM-BSE images showing only ferrite and austenite ($T_p = 1350\ °C$): (a) S32205; (b) S32750

**Table 4** $\Delta t_{12/8}$ and cooling rate from 1200 to 800 °C in the thermal cycles imposed in the Gleeble HAZ simulation with $T_P = 1200$ and 1350 °C

| Steel | $\Delta t_{12/8}$, s | | Average cooling rate, °C/s | |
|---|---|---|---|---|
| | $T_P = 1200\ °C$ | $T_P = 1350\ °C$ | $T_P = 1200\ °C$ | $T_P = 1350\ °C$ |
| S32205 | 46.0 | 41.0 | 8.7 | 9.8 |
| S32750 | 55.3 | 41.5 | 7.2 | 9.6 |

than 1000 °C show a trend of CPT decrease. This is mainly due to the increase in chromium nitride precipitation, as shown in Fig. 8(a-d) and Fig. 9(a) and (b). The lowest pitting corrosion resistances in both steels were found in specimens with peak temperature 1350 °C, and this result can be associated to the microregion of real welded joints where the peak temperature is high enough to produce an excess of ferrite and intense chromium nitrides precipitation.

Specimens of duplex S32205 with $T_P = 1350\ °C$ and superduplex S32750 with $T_P = 1200\ °C$ were selected to perform cyclic polarization tests in 3.5%NaCl solution at temperatures above the CPT (60 °C for DSS and 80 °C for SDSS). Figure 14(a) and (b) shows the polarization curves. The pitting potentials indicated are very low because the tests were performed above the CPT. In both steels, the pits were found to nucleate preferentially in the ferrite ($\alpha$) phase, and in the $\alpha/\gamma$ boundaries, as shown in Fig. 15(a), (c) and (d). Figure 15(b) shows a large pit growing through the $\alpha$ phase, preserving austenitic islands. The preferential pit nucleation and growth in the ferrite phase may be attributed to chromium nitrides precipitated in this phase and in the $\alpha/\gamma$ boundaries.
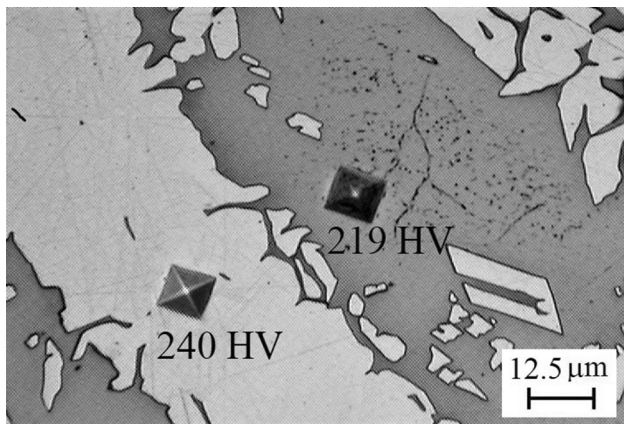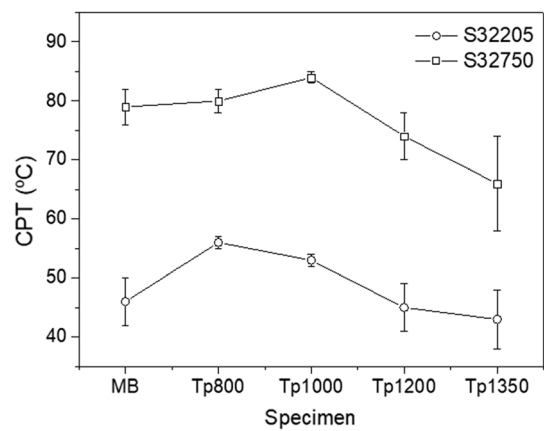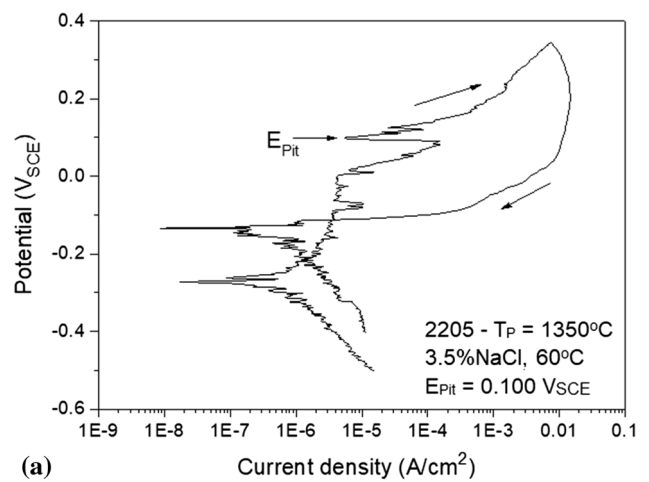
(a)



**Fig. 13** CPT results as function of the $T_P$
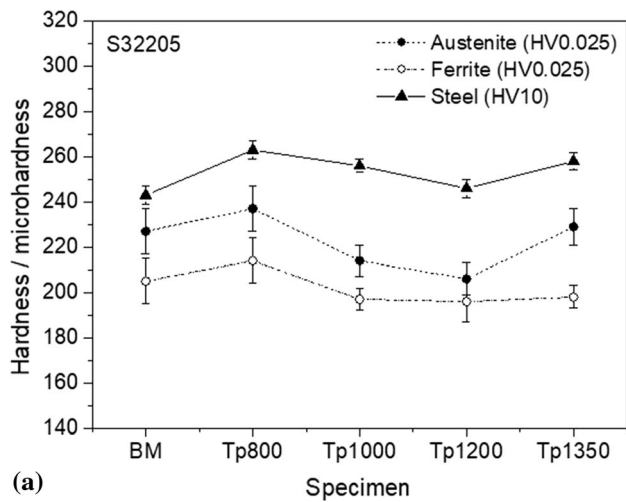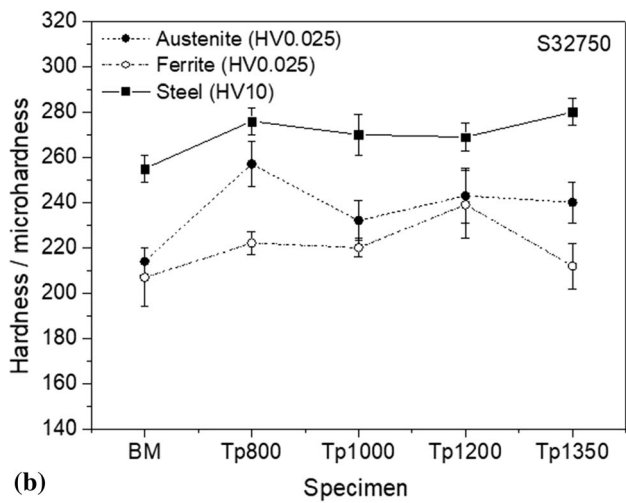


(b)

**Fig. 11** Hardness and microhardness of ferrite and austenite: (a) S32205; (b) S32750
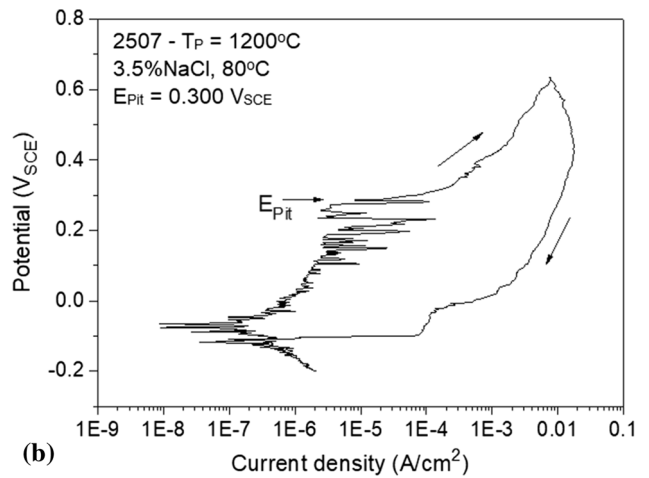


219 HV

240 HV

12.5 µm

**Fig. 12** Comparison of microhardness indentations in ferrite (dark) and austenite (light) in steel S32750 processed with $T_P$ = 1350 °C



$E_{Pit}$

2205 - $T_P$ = 1350°C
3.5%NaCl, 60°C
$E_{Pit}$ = 0.100 $V_{SCE}$

(a)



2507 - $T_P$ = 1200°C
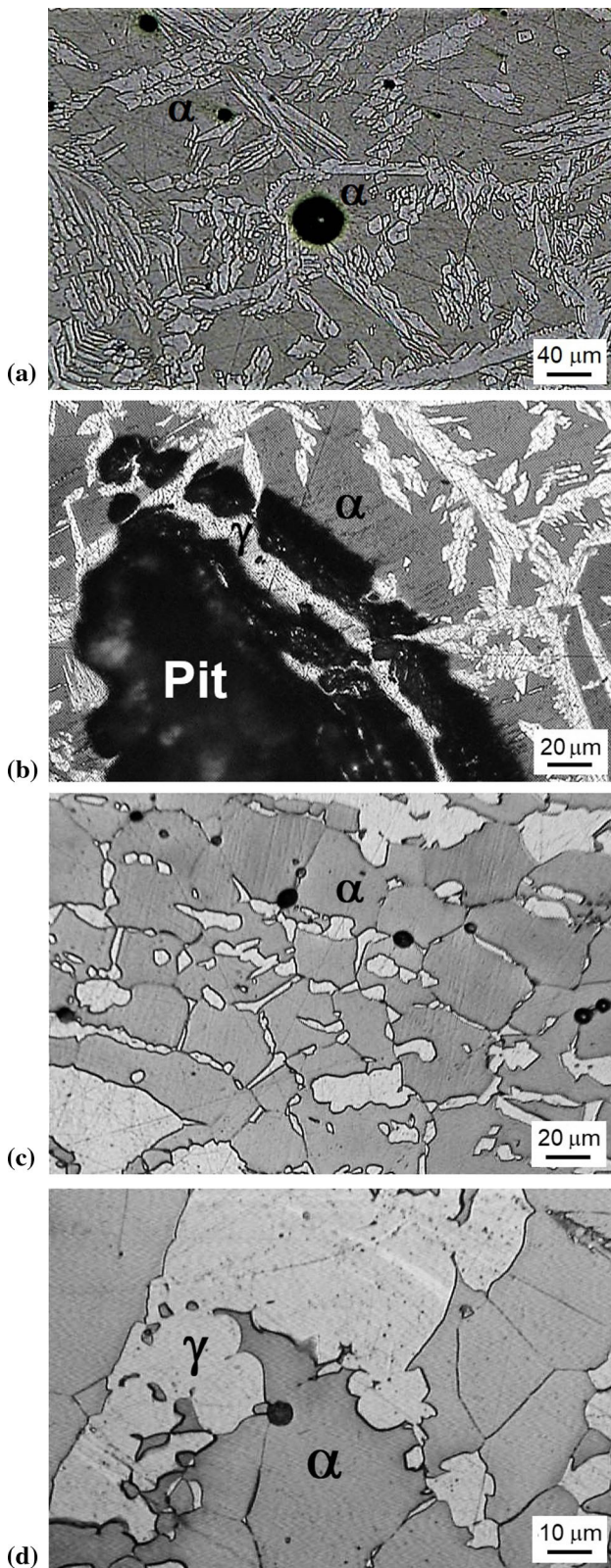3.5%NaCl, 80°C
$E_{Pit}$ = 0.300 $V_{SCE}$

$E_{Pit}$

(b)

**Fig. 14** Cyclic polarization curves in 3.5%NaCl solution: (a) S32205, 60 °C; (b) S32750, 80 °C

**Fig. 15** Pits observed in the microstructure after the polarization tests: (a) and (b) S32205; (c) and (d) S32750

# 4. Conclusions

Specimens of duplex (UNS S32205) and superduplex (UNS S32750) steels were submitted to Gleeble thermal simulation of the heat-affected zone, with peak temperatures ($T_P$) 800, 1000, 1200 and 1350 °C. The main conclusions are:

- The duplex S32205 steel has a higher ferritizing tendency than the superduplex S32750 due to its higher $Cr_{eq}/Ni_{eq}$ ratio.
- Intense Cr nitrides precipitation occurs in the specimens processed with $T_P$ = 1350 °C, and, to a less extent, in specimens processed with $T_P$ = 1200 °C. The chromium nitride precipitation is restricted to the ferrite but does not promote the hardening of this phase.
- The HAZ simulated with $T_P$ = 1200 and 1350 °C had a $\Delta t_{12/8}$ between 41 and 53 s, but this cooling time did not provoke sigma ($\sigma$) or chi ($\chi$) precipitation.
- The intense Cr nitride precipitation provoked the decrease in the critical pitting temperature (CPT) in specimens of HAZ simulated with peak temperatures of 1200 and 1350 °C.
- The ferrite ($\alpha$) phase and the $\alpha/\gamma$ boundaries are preferential sites for pit nucleation, as observed in cyclic polarization tests of specimens processed with peak temperatures 1350 and 1200 °C.

## References

1. J.-O. Nilsson, Super Duplex Stainless Steels, *Mater. Sci. Technol.*, 1992, **8**(8), p 685–700
2. IMOA, in *Practical Guidelines for the Fabrication of Duplex Stainless Steels*, 2nd edn. (International Molybdenum Association (IMOA), 2009)
3. R.N. Gunn, *Duplex Stainless Steels: Microstructure, Properties and Applications*, 1st ed. Abington Publishing, 1997
4. Yt. Shin, Hs. Shin and Hw. Lee, Effects of Heat Input on Pitting Corrosion in Super Duplex Stainless Steel Weld Metals, *Met. Mater. Int.*, 2012, **18**(6), p 1037–1040
5. A. Corolleur, A. Fanica and G. Passot, Ferrite Content in the Heat Affected Zone of Duplex Stainless Steels, *Berg Huettenmaenn Monatsh*, 2015, **160**(9), p 413–418
6. API, API RP 582-2009. *Welding Guidelines for the Chemical, Oil, and Gas Industries* (American Petroleum Institute, 2009)
7. API, API TR 938-C-2015. *Use of Duplex Stainless Steels in the Oil Refining Industry* (American Petroleum Institute, 2015)
8. NORSOK, *M-630 Material Data Sheets and Element Data Sheets for Piping* (Standards Norway, 2013)
9. G.R. Hitchcock, W.F. Deans, D.S. Thompson and A. Coats, Pin-Hole and Crack Formation in a Duplex Stainless Steel Downhole Tool, *Eng. Fail. Anal.*, 2001, **8**(3), p 213–226
10. J. Smiderle, J.M. Pardal, S.S.M. Tavares and A.C.N. Vidal, Premature Failure of Superduplex Stainless Steel Pipe by Pitting in Sea Water Environment, *Eng. Fail. Anal.*, 2014, **46**, p 134–139

11. V.M. Linton, N.J. Laycock, S.J. Thomsen and A. Klumpers, Failure of a Super Duplex Stainless Steel Reaction Vessel, *Eng. Fail. Anal.*, 2004, **11**(2), p 243–256

12. L. Li, Z. Du, X. Sheng, M. Zhao, L. Song, B. Han and X. Li, Comparative Analysis of GTAW+SMAW and GTAW Welded Joints of Duplex Stainless Steel 2205 Pipe, *Int. J. Press. Vessels Pip.*, 2022, **199**, p 104748

13. H.B. Pereira, T.H.C. Pimentel, C.A. da Silva, Z. Panossian and C.R.F. de Azevedo, Influence of Welding Energy on Intergranular and Pitting Corrosion Susceptibility of UNS S32205 Duplex Stainless-Steel Joints, *Mat. Res.*, 2022, **25**(suppl 1), p e20210488

14. S.S.M. Tavares, J.M. Pardal, L.D. Lima, I.N. Bastos, A.M. Nascimento and J.A. de Souza, Characterization of Microstructure, Chemical Composition, Corrosion Resistance and Toughness of a Multipass Weld Joint of Superduplex Stainless Steel UNS S32750, *Mater. Charact.*, 2007, **58**(7), p 610–616

15. M.C. Young, S.L.I. Chan, L.W. Tsay and C.-S. Shin, Hydrogen-Enhanced Cracking of 2205 Duplex Stainless Steel Welds, *Mater. Chem. Phys.*, 2005, **91**(1), p 21–27

16. S.S.M. Tavares, C. Scandian, J.M. Pardal, T.S. Luz and F.J. da Silva, Failure Analysis of Duplex Stainless Steel Weld Used in Flexible Pipes in off Shore Oil Production, *Eng. Fail. Anal.*, 2010, **17**(6), p 1500–1506

17. S.S.M. Tavares, J.M. Pardal, L.F. Noris and M.G. Diniz, Microstructural Characterization and Non-destructive Testing and of Welded Joints of Duplex Stainless Steel in Flexible Pipes, *J. Mater. Res. Technol.*, 2021, **15**, p 3399–3408

18. L. Pezzato, M. Lago, K. Brunelli, M. Breda and I. Calliari, Effect of the Heat Treatment on the Corrosion Resistance of Duplex Stainless Steels, *J. Mater. Eng. Perform.*, 2018, **27**(8), p 3859–3868

19. M. Knyazeva and M. Pohl, Duplex Steels. Part II: Carbides and Nitrides, *Metallogr. Microstruct. Anal.*, 2013, **2**(5), p 343–351

20. N. Pettersson, R.F.A. Pettersson and S. Wessman, Precipitation of Chromium Nitrides in the Super Duplex Stainless Steel 2507, *Metall. Mater. Trans. A*, 2015, **46**(3), p 1062–1072

21. C. Gennari, M. Lago, B. Bögre, I. Meszaros, I. Calliari and L. Pezzato, Microstructural and Corrosion Properties of Cold Rolled Laser Welded UNS S32750 Duplex Stainless Steel, *Metals*, 2018, **8**(12), p 1074

22. E.V. Morales, J.A. Pozo, L. Olaya, E. Kassab, J.A.C. Ponciano, K. Ghavami and I.S. Bott, Remarks on the Evolution and Performance of the Different Austenite Morphologies at the Simulated HAZs of a 2205 Duplex Stainless Steel, *J. Mater. Res. Technol.*, 2019, **8**(5), p 3936–3949

23. R.-I. Hsieh, H.-Y. Liou and Y.-T. Pan, Effects of Cooling Time and Alloying Elements on the Microstructure of the Gleeble-Simulated Heat-Affected Zone of 22% Cr Duplex Stainless Steels, *J. Mater. Eng. Perform.*, 2001, **10**(5), p 526–536

24. ASTM, *A790/A790M Standard Specification for Seamless and Welded Ferritic/Austenitic Stainless Steel* (ASTM International, 2020)

25. N.N. Rykalin, in *Calculation of Heat Processes in Welding* (Moscow, 1960)

26. ASTM, *G150-Standard Test Method for Electrochemical Critical Pitting Temperature Testing of Stainless Steels* (ASTM International, 2018) https://doi.org/10.1520/G0150-18

27. J.N. Conceição, E.O. Correa, A.C. Gonzaga, J.M. Pardal and S.S.M. Tavares, Mechanical Properties of UNS S39274 Superduplex Stainless Steel Work Hardened and Solution Annealed, *Mater. Res.*, 2022, **25**, p e20220108

28. J.C. Lippold and D.J. Kotecki, *Welding Metallurgy and Weldability of Stainless Steels*, John Wiley and Sons, 2005

29. S.M. Kim, J.S. Kim, K.T. Kim, K.-T. Park and C.S. Lee, Effect of Ce Addition on Secondary Phase Transformation and Mechanical Properties of 27Cr-7Ni Hyper Duplex Stainless Steels, *Mater. Sci. Eng. A*, 2013, **573**, p 27–36

30. S.-H. Jeon, S.-T. Kim, I.-S. Lee, J.-S. Kim, K.-T. Kim and Y.-S. Park, Effects of W Substitution on the Precipitation of Secondary Phases and the Associated Pitting Corrosion in Hyper Duplex Stainless Steels, *J. Alloy. Compd.*, 2012, **544**, p 166–172

31. S. Hereñú, M.G. Moscato, I. Alvarez and A.F. Armas, The Influence of Chromium Nitrides Precipitation on the Fatigue Behavior of Duplex Stainless Steels, *Procedia Eng.*, 2014, **74**, p 179–182

32. W. Horvath, B. Tabernig, E. Werner and P. Uggowitzer, Microstructures and Yield Strength of Nitrogen Alloyed Super Duplex Steels, *Acta Mater.*, 1997, **45**(4), p 1645–1654

33. S.S.M. Tavares, A. Loureiro, J.M. Pardal, T.R. Montenegro and V.C. da Costa, Influence of Heat Treatments at 475 and 400 °C on the Pitting Corrosion Resistance and Sensitization of UNS S32750 and UNS S32760 Superduplex Stainless Steels, *Mater. Corros.*, 2011 https://doi.org/10.1002/maco.201006016